Published August 10, 2016, doi:10.4049/jimmunol.1600628

Systems Analysis of the Complement-Induced Priming Phase of Liver Regeneration

Jun S. Min,* Robert A. DeAngelis,† Edimara S. Reis,† Shakti Gupta,* Mano R. Maurya,* Charles Evans,‡ Arun Das,‡ Charles Burant,‡ John D. Lambris,† and Shankar Subramaniam§,¶,‖,#

Liver regeneration is a well-orchestrated process in the liver that allows mature hepatocytes to reenter the cell cycle to proliferate and replace lost or damaged cells. This process is often impaired in fatty or diseased livers, leading to cirrhosis and other deleterious phenotypes. Prior research has established the role of the complement system and its effector proteins in the progression of liver regeneration; however, a detailed mechanistic understanding of the involvement of complement in regeneration is yet to be established. In this study, we have examined the role of the complement system during the priming phase of liver regeneration through a systems level analysis using a combination of transcriptomic and metabolomic measurements. More specifically, we have performed partial hepatectomy on mice with genetic deficiency in C3, the major component of the complement cascade, and collected their livers at various time points. Based on our analysis, we show that the C3 cascade activates c-fos and promotes the TNF-α signaling pathway, which then activates acute-phase genes such as serum amyloid proteins and orosomucoids. The complement activation also regulates the efflux and the metabolism of cholesterol, an important metabolite for cell cycle and proliferation. Based on our systems level analysis, we provide an integrated model for the complement-induced priming phase of liver regeneration. ***The Journal of Immunology*****, 2016, 197: 000–000.**

The liver is the second largest organ in the body with the unique ability to regenerate itself from as little as 25% of its original mass (1, 2). This regenerative property is essential in supporting the ongoing central role of the liver in many biological processes such as complex homeostasis and compound detoxification. However, liver regeneration is impaired in diseased, aged, or fatty livers (3–7). Therefore, a detailed understanding of the mechanisms underlying liver regeneration is necessary for the development of therapies to enhance or restore the regenerative property of livers in which it is impaired. Despite many efforts to unravel the mechanisms of liver regeneration over the past decades, the complex mechanisms still have not been fully mapped (8).

Liver regeneration occurs in three main phases: priming, proliferation, and termination (9). During the priming phase of liver regeneration, which lasts ∼4 h in mice, the majority of quiescent hepatocytes rapidly reenter the cell cycle with the help of various cytokines such as TNF-α and IL-6 (9, 10). These cytokines are mainly produced by nearby liver macrophages, also known as Kupffer cells, that are activated by LPS and complement effector proteins such as C3a and C5a (11). The proliferation phase occurs when hepatocytes undergo mitosis, with the expansion of the remaining liver occurring with the help of growth factors and metabolic signaling (12). In rodents, most of the increase in the liver mass occurs by day 3 after surgical resection of two thirds of the liver, called partial hepatectomy (PHx), with complete mass restoration achieved by 5–7 d postsurgery (12, 13). Finally, the termination phase occurs with the regulation of various pathways that can alter the hepatic mass (14). Of the main stages of liver regeneration, the priming phase is of great interest because the normally quiescent hepatocytes reenter the cell cycle to proliferate in response to an injury or an infection (12). A better understanding of this phase of liver regeneration can provide key insights into the complex pathways that activate cellular proliferation and facilitate interventions to accelerate liver regeneration.

*Department of Bioengineering, University of California, San Diego, La Jolla, CA 92093; †Department of Pathology and Laboratory Medicine, University of Pennsylvania, Philadelphia, PA 19104; ‡Department of Computational Medicine and Bioinformatics, University of Michigan Medical School, Ann Arbor, MI 48109; §Graduate Program in Bioinformatics, Department of Computer Science and Engineering, University of California San Diego, La Jolla, CA 92093; ¶Department of Bioengineering, Institute of Engineering in Medicine, University of California, San Diego, La Jolla, CA 92093; ‖Department of NanoEngineering, University of California, San Diego, La Jolla, CA 92093; and #Department of Cellular and Molecular Medicine, University of California, San Diego, La Jolla, CA 92093

ORCIDs: 0000-0001-6380-3351 (J.S.M.); 0000-0002-8438-275X (E.S.R.); 0000-0003-4249-067X (M.R.M.); 0000-0001-6698-5330 (C.E.); 0000-0002-0883-1816 (A.D.); 0000-0001-9189-5003 (C.B.); 0000-0002-8059-4659 (S.S.).

Received for publication April 12, 2016. Accepted for publication July 12, 2016.

This work was supported by National Institutes of Health Grants U01 DK097430, R01HL106579 and R01HL108735 (to S.S.), and AI068730 (to J.D.L.). This work also used Core Services supported by National Institutes of Health Grant DK097153 (to the University of Michigan).

S.S. and J.D.L. conceived and supervised the project; most of the analyses were carried out by J.S.M. with assistance from S.G. and M.R.M.; R.A.D. and E.S.R. carried out the animal experiments and RNA extraction, whereas the mass spectrometric study was carried out in the University of Michigan Core by C.E. and A.D. with supervision by C.B.; the draft of the manuscript was written by J.S.M. and was reviewed by all authors and revised by J.D.L. and S.S.

Address correspondence and reprint requests to Dr. Shankar Subramaniam or Dr. John D. Lambris, Department of Bioengineering, University of California San Diego, 9500 Gilman Drive #0412, La Jolla, CA 92093 (S.S.) or University of Pennsylvania, 401C Stellar-Chance Building, 422 Curie Boulevard, Philadelphia, PA 19104 (J.D.L.). E-mail addresses: shankar@ucsd.edu (S.S.) or lambris@upenn.edu (J.D.L.)

The online version of this article contains supplemental material.

Abbreviations used in this article: ABCG, ATP-binding cassette subfamily G; CE, cholesterol ester; DAVID, Database for Annotation, Visualization and Integrated Discovery; FAME, fatty acid methyl ester; FDR, false-discovery rate; GC, gas chromatography; HDL, high-density lipoprotein; HMG, 3-hydroxy-3-methylglutaryl; HMGCR, HMG-CoA reductase; KO, knockout; LXR, liver X receptor; MS, mass spectrometry; ORM, orosomucoid; PHx, partial hepatectomy; PL, phospholipid; qPCR, quantitative PCR; SAA, serum amyloid A; SOCS3, suppressor of cytokine signaling 3; TLC, thin-layer chromatography; WT, wild-type.

The complement system is part of the innate immune system and has recently been introduced as one of the key regulators of liver regeneration (11, 15–17). In prior studies, complement knockout (KO) mice were used to demonstrate the importance of the complement effector proteins, C3a and C5a, in mediating successful liver regeneration (16, 17). Mice deficient in C3 and C5 genes exhibited severe damage to parenchyma, increased necrosis and hepatocyte degeneration, and higher mortality than wild-type (WT) controls during liver regeneration (16–18). Various inflammatory cytokines and pathways were significantly affected in the complement KO mice, especially during the first few hours after PHx (17, 18). Based on these studies, an overall mechanism of complement-induced liver regeneration with a focus on intercellular signaling has been proposed (11).

In this study, we report additional insights into liver regeneration through a comparative time-course analysis of transcriptional and metabolic changes in WT and C3 KO mice during the priming phase. Our analysis shows the role of acute-phase proteins and the modulation of regeneration by sterol metabolism.

Materials and Methods

Animal studies

PHx experiments, according to the method of Higgins et al. (19), were performed to remove two thirds of the liver from 13- to 16-wk-old male mice of either C57BL/6 WT or $C3^{-/-}$ (KO) origin. Only male mice were chosen because of the reported findings that suggest sex differences can exist in liver regeneration (20, 21). Age- and sex-matched WT and KO mice underwent sham surgery to serve as negative controls. These sham experiments were necessary because surgical inflammation can influence the expression of genes related to the cell cycle or proliferation, which would interfere with the analysis of the priming phase of liver regeneration that is dependent on these biological processes. After the PHx experiments, the remaining parts of the liver were collected after 0.5, 1, and 3 h to capture temporal changes during the priming phase of liver regeneration. Livers were also collected from WT and KO mice without surgery at 0 h to assess baseline difference. Whole livers, instead of isolated hepatocytes, were analyzed in the study because the experimental process of separation is not only difficult but also known to cause stress signals to the cells, which would complicate the early inflammatory signals. Three biological replicates were used for each PHx and sham experiment for each group to account for biological variability.

RNAseq experiments

From the collected livers at various time points, RNA was extracted and purified with a Qiagen Allprep Kit for cDNA synthesis and gene expression analysis. A pooling scheme was devised to reduce the number of samples to 21 (Supplemental Table I). The pooled RNA samples were run on a Bioanalyzer to check for their RNA integrity. An Illumina Truseq cDNA library construction kit was used to synthesize cDNA libraries after poly-A selection and fragmentation. Then the cDNA fragments were size-selected and inserted into the flow cell of a HisEquation 2000 at the Biogem facility of the University of California, San Diego. The sequencing option was single-end 50-bp with seven samples in each of the three lanes.

RNAseq pipeline

An RNAseq pipeline was developed with existing tools to effectively analyze the transcriptomic data. First, Omicsoft Sequence Aligner was used to align the RNAseq reads to the mouse genome and the transcriptome with the default parameters (22). Then HTseq-count was used to quantify the number of aligned reads associated with each gene and transcript (23). All uniquely mapped reads were counted, but ambiguous reads that mapped to several different genes were ignored. DESeq, a popular R package for RNAseq analysis, was used to derive the list of differentially expressed genes across paired conditions (24). Different combinations of parameters and filtering schemes were optimized to produce the highest number of statistically relevant genes. For example, the genes in the lowest 40% quantile of the total read counts across all samples were removed to increase the power of the statistical analysis whereas minimizing the removal of differentially regulated genes. The counted reads were normalized with the DESeq's default method, whereas the variance was estimated for each condition. The statistical tests were performed on each of the seven core groups between PHx and sham: KO versus WT at 0 h, KO PHx versus KO sham at 0.5 h, KO PHx versus KO sham at 1 h, KO PHx versus KO sham at 3 h, WT PHx versus WT sham at 0.5 h, WT PHx versus WT sham at 1 h, and WT PHx versus WT sham at 3 h. Once the p values and the false-discovery rate (FDR) values from the Benjamini-Hochberg method were calculated for each gene in the core groups, the genes less than either the FDR of 0.1 or the p value of 0.05 were chosen for further analyses.

In addition to the statistical tests performed on PHx versus sham, the sequential fold change cutoff of 1.5 was applied to create the list of differentially upregulated or downregulated genes in the KO mice with respect to the WT. More specifically, the union of differentially regulated genes from the statistical tests in the KO and the WT livers was obtained at each time point. Then, from the combined list of genes, only the genes with the KO/WT fold change difference of $\geq$1.5 were selected. Both the KO and the WT PHx expression levels were normalized with respect to sham from the previous DESeq analysis. As a result, the final list of differentially regulated genes in the KO, which also show significant differences with respect to sham, was generated. For the differential analysis at 0 h, only the DESeq results with the p value cutoff of 0.05 were used between the KO and the WT samples. The complete workflow to derive the list of differentially regulated genes at each time point is shown in the Supplemental Table II.

Quantitative PCR experiments

The genes, c-fos, c-jun, and TIS21, which showed the greatest changes over time with respect to sham control during the priming phase of liver regeneration from the study by Su et al. (10), were selected for quantitative PCR (qPCR) validation. GAPDH was used as the housekeeping gene. The primer sequences for the genes were obtained from the published studies and Primerbank, Harvard online database for PCR primers that have been validated for mouse genes (25, 26). The primer sequences are listed as follows: 5′-CCTTCGGATTCTCCGTTTCTCT-3′ (forward) and 5′-TGGTGAAGACCGTGTCAGGA-3′ (reverse) for c-fos; 5′-CCTTCTACGACGATGCCCTC-3′ (forward) and 5′-GGTTCAAG GTCATGCTCTGTTT-3′ (reverse) for c-jun; 5′-ATGAGCCACGGGAA-GAGAAC-3′ (forward) and 5′-GCCCTACTGAAAACCTTG AGTC-3′ (reverse) for TIS21; 5′-AGGTCGGTGTGAACGGATTTG-3′ (forward) and 5′-TGTAGACCATGTAGTTGAGGTCA-3′ (reverse) for GAPDH. Before the qPCR experiments, a set of validation experiments was performed to test the primers and check their PCR efficiencies for 4-log dilution. The qPCR experiments were performed in two steps. First, the cDNA library was created from the purified RNAs using a High-Capacity cDNA Reverse Transcription Kit from Applied Biosystems. Then, the cDNA library was mixed with each of the four primers and Fast SYBR Green Master Mix from Applied Biosystems. Real-time fluorescent measurements were taken from the Eppendorf RealPlex qPCR machine. For each biological replicate, three technical replicates were used.

Enrichment analysis

Database for Annotation, Visualization and Integrated Discovery (DAVID) analysis was performed to identify significantly enriched Kyoto Encyclopedia of Genes and Genomes pathways and biological processes from Gene Ontology terms under the modified Fisher exact p value cutoff of 0.05 (27). A heat map was derived for the enrichment results with Circos software (28). Negative $\log_2$ of enrichment p value was used as the scale for the heat map.

Network analysis

An integrative analysis using protein–protein interactions and gene expression data were performed by using a custom mouse interaction network derived in Cytoscape, a network visualization tool (29). This mouse interaction network was derived from the known mouse protein–protein interactions and transcription factor-to-target interactions using online databases such as STRING, BIOGRID, and TRANSFAC (30–33). From the STRING database that uses a scoring scheme between 0 and 1 based on both predicted and experimentally validated protein–protein interactions, a 0.9 cutoff was used to extract highly feasible protein–protein interactions. Autosome clustering from the Clustermaker plugin of Cytoscape was used to identify the clusters of genes that are well-connected within the mouse interaction network (34, 35). Autosome clustering uses the unsupervised training of a self-organizing map, a type of artificial neural network in machine learning (35). This algorithm used correlation from the gene expression data as node weights to find the clusters of genes that are different from each other. Among these clusters that are separated from one another, the largest clusters with enriched biological functions or Kyoto Encyclopedia of Genes and Genomes pathways were selected as relevant networks for further analyses.

Metabolomics

Mass spectrometry (MS) measurements were made for 143 metabolites for all 3 biological replicates for each genotype, time point, and experiment (sham, PHx). The measured metabolites included cholesterol esters (CEs), phospholipids (PLs), and metabolites in the sterol pathway (Supplemental Material List). The PHx values were first normalized with respect to their sham control. Then the final fold change between the KO and the WT was calculated by comparing their normalized PHx values. The MS measurements of important metabolites were used together with the transcriptomic data to identify novel mechanisms and derive mechanistic insights.

Sterol pathway metabolite analysis

Frozen tissues were extracted in a similar manner as described previously (36). In brief, frozen tissue samples were pulverized using a liquid nitrogen-chilled mortar and pestle; then a 30-mg portion of the pulverized frozen tissue was extracted by sonication with 1 ml of 7:2:1 methanol: water:chloroform containing stable isotope-labeled internal standards: $[^{13}C]_{10}[^{15}N]_5$ adenosine monophosphate, $[^{13}C]_4$ malate, and $[^{13}C]_6$ citrate at 200, 200, and 20 μM, respectively. After centrifugation, two 200 μl aliquots of supernatant were reserved for liquid chromatography-MS and gas chromatography (GC)-MS analysis of sterol synthesis intermediates. The liquid chromatography-MS analysis was performed using an Agilent 1200 LC instrument connected to an Agilent 6410 tandem quadrupole MS. Chromatography was performed using a Phenomenex Luna NH_2 column. Mobile phase A was acetonitrile and mobile phase B was 5 mM ammonium acetate in water, adjusted to pH 9.9 with ammonium hydroxide. The gradient consisted of a linear ramp from 20 to 100% B over 15 min, followed by a 5-min hold and a 15-min re-equilibration period at 100% B. The flow rate was 0.07 ml/min and the injection volume was 40 μl. MS was performed using negative ion electrospray ionization in multiple reaction monitoring mode. Metabolite identification in biological samples was performed based on matching retention times and MS/MS transitions determined using authentic standards (Supplemental Table III). Quantitation was performed based on calibration curves generated using authentic standards, and all metabolite peak areas were normalized to the peak area of the internal standard with closest-matching retention time. Internal standards were included at identical concentrations in both samples and standards.

For GC-MS analysis, the 200 μl aliquot of muscle extract supernatant was dried in a glass vial under a gentle stream of nitrogen gas, then derivatized using a two-step procedure similar to one described previously (37). First, 30 μl of 20 mg/ml methoxyamine hydrochloride in pyridine was added to the dried sample and heated at 37˚C for 1 h. Then, 30 μl of *N*-methyl-*N*-(trimethylsilyl)trifluoroacetamide with 1% trimethylchlorosilane was added to the sample and heated at 70˚C for 1 additional hour. The resulting derivatized sample was analyzed by GC-MS on an Agilent 7890 GC with a 5975 mass spectrometer. The instrument was equipped with an Agilent HP-5MS column. The temperature program consisted of 1 min initial time at 80˚C, a 10-min ramp from 80 to 320˚C, and a 1-min hold at 320˚C for 12 min total run time. Other parameters were as follows: 250˚C inlet temperature, 1 μl injection volume, splitless injection mode, helium carrier gas, 1.4 ml/min constant column flow rate, scan, m/z 40–650 MS mode. Peaks were putatively identified by searching against the NIST 2011 and Fiehn 2013 spectral libraries followed by manual confirmation of spectral similarity. Peak areas were used for relative quantitation of metabolite levels.

Lipid extraction and fatty acid profiling of total PLs and CEs

Lipids were extracted from frozen pulverized tissues (20–25 mg) following essentially Bligh and Dyer's method of solvent partition (38). A typical extraction procedure consists of suspending the tissues in 0.6 ml of water followed by adding 2.25 ml of a mixture of chloroform-methanol (1:2) containing 0.01% BHT and 10 μl of 4 mM heptadecanoic acid (C17:0) as an internal standard. The mixture was homogenized with a Polytron homogenizer. The homogenized samples were further treated with 0.75 ml each of chloroform and NaCl (0.9%) solution followed by mixing and centrifugation at ~3000 rpm for 5–6 min on a tabletop centrifuge. The lower organic chloroform layer containing the lipids was separated out and saved at −20˚C unless used as follows.

Isolation of total PLs and CEs by thin-layer chromatography

The solvents from the lipid extracts were removed under nitrogen and redissolved in a small volume of chloroform for chromatography on thin-layer chromatography (TLC) plate (silica gel 60; Merck, Germany). The samples were applied as a band on the plate applying side by side standard PL and CE as reference spots. The plate was developed with a solvent mixture of hexane-diethyl ether-acetic acid (80-20-1.5, v/v). Total PLs and CEs were then identified by comparing the retention flow of the authentic standards. The lipid contents from the TLC powders were extracted with chloroform followed by removal of the solvents under nitrogen and subject to transmethylation as follows.

Preparation of methyl ester with boron trifluoride-methanol

The fatty acid components of the lipids were derivatized into their methyl esters using boron trifluoride-methanol (39). To the dry residue, 2 ml of boron trifluoride-methanol, 14% solution from Sigma, was added; the tubes containing the mixture were closed under nitrogen and incubated at 60˚C for ~3–3.5 h. The methyl esters were extracted by adding 2 ml of hexane and 1 ml of water, with mixing and then centrifuging followed by collection in the upper hexane layers. A TLC purification step was necessary for the methyl ester derived from CE to remove liberated free cholesterol before GC analysis. A similar TLC procedure as described earlier was performed applying standard fatty acid methyl ester (FAME) for identification purposes. The identified FAMEs were extracted from the TLC powder with hexane, the volumes were concentrated appropriately, and the fatty acid compositions of CEs and total PLs were analyzed by GC.

Analysis of CE and PL-derived FAMEs by GC

Analysis of FAMEs was performed by GC on an Agilent GC model 6890N equipped with flame ionization detector, an autosampler, and ChemStation software for data analysis. The GC column used was Agilent HP 88, 30 m, 0.25 mm inner diameter, and 0.20-μm film thickness. Hydrogen was used as a carrier gas as well as for the flame ionization detector, and nitrogen was used as a makeup gas. Analyses were carried out with a temperature program of 125–220˚C. A calibration curve was prepared using proportional amounts of C17:0 methyl ester standard. A mixture of standard methyl esters was also run to identify the components in unknown samples by comparing their retention times. The fatty acids were quantified with respect to the amounts of C17:0 internal standard added and the calibration curve prepared. The coefficient of variation for GC analyses was found to be within 2.5 to 3.6%.

Correlational analysis

Pearson correlation analyses were performed in Excel. The first correlation analysis compared cytokine and transcriptomic profiles. Correlation between our previously published cytokine data and the acute-phase genes was performed with a time delay; the cytokine measurements at 0, 0.5, and 1 h were compared with the gene expression measurements at 0.5, 1, and 3 h, respectively (18). The second correlation analysis compared the transcriptomic and the metabolic data in the sterol pathway at the same time points. The expanded pathway for sterol lipids was taken from LIPID Metabolites and Pathways Strategy (40, 41). In the sterol pathway, multiple genes regulated certain metabolites; among these genes, only the gene with the highest correlation with its paired metabolite was selected. The second correlation analysis used three time points (0.5, 1, and 3 h) for the KO and the WT, and four time points (0, 0.5, 1, and 3 h) for the KO/WT fold change. The correlation results in the sterol pathway were visualized through a heat map.

Results

Transcriptional changes

To explore the molecular events in the priming phase of complement-induced liver regeneration, we first analyzed the time-series transcriptomic data in the C3 KO and the C57BL/6 WT livers using RNAseq across multiple conditions (Supplemental Table I). The alignment result from the RNAseq experiments produced the following statistics: aside from one outlier, the samples had an average count of 15 million uniquely mapped reads, 3 million of which were splice reads (Supplemental Table IV). Correlation between the RNAseq and the qPCR data for the selected genes, c-fos, c-jun, and TIS21, was high ($r^2 = 0.76$; Supplemental Fig. 1).

To identify differentially regulated genes, we first performed differential analysis using DEseq on PHx versus sham for every genotype and time point to account for the inflammatory effect from the surgery. Then, a fold change cutoff of 1.5 was applied between the KO and the WT to produce the final list of differentially regulated genes. The total numbers of differentially regulated genes are shown in Fig. 1A and 1B. The results showed an increase in the number of differentially regulated genes primarily at 3 h after PHx, suggesting

that a small set of genes, such as immediate early genes and transcription factors, are influenced first, with their downstream genes subsequently regulated.

Activation of multiple signaling pathways

The complement system has been shown to increase the production of IL-6 and TNF-α, which play a key role in liver regeneration by activating signaling pathways such as the NF-κB pathway in Kupffer cells (11). We confirmed that the signaling pathways activated by these cytokines in hepatocytes are deactivated in the KO mice. For example, differentially regulated genes showed enrichment in inflammatory and cell cycle–related pathways, such as JAK-STAT, MAPKs, and TGF-β, demonstrating that the complement system activates an acute-phase, proliferative response between 1 and 3 h after liver injury (Fig. 1C). We also observed an indication of metabolic changes in the KO transcriptome; retinol metabolism, cholesterol biosynthetic processes, peroxisome proliferator-activated receptors, and the insulin signaling pathways were significantly enriched at 0 and 3 h after PHx (Fig. 1C).

Temporal network analysis

To investigate the complex temporal changes in the transcriptome, we created networks in Cytoscape at each time point (Fig. 2). These networks were derived from the gene expression data and a custom mouse interaction network composed of protein–protein and transcription factor interactions (see *Materials and Methods*). Autosome clustering was applied to create clusters, or networks of genes, that were different from each other based on transcriptomic coexpression values. The largest and the most statistically significant network of genes that is enriched with transcription factors and cell cycle–related genes ($p < 0.05$) is shown at each time point (Fig. 2). Other networks of genes from the clustering method were small and did not provide significant biological insights. The temporal network analysis revealed progressive downregulation of c-fos in the KO. It also revealed a significant, transient upregulation of suppressor of cytokine signaling 3 (SOCS3) and STAT3 in the first hour. Besides these clear changes in recognized genes, other changes in the transcriptional network across the multiple time points were complex, emphasizing the intricate regulation of multiple transcription factors and their target genes by the complement system during the priming phase of liver regeneration.

Complement and the acute-phase response

The acute-phase response was one of the most significantly overrepresented biological processes in the KO across many time points from the enrichment analysis (Fig. 1C). Therefore, we analyzed the transcriptional regulation of the acute-phase genes from the acute-phase response signaling pathway from QIAGEN's Ingenuity Target explorer (42) (Fig. 3). Among the acute-phase genes, serum amyloid A (SAA) and orosomucoid (ORM) genes showed significant transcriptional regulation and similar temporal patterns with a progressive decline in expression in the KO livers from 0.5 to 3 h, whereas their WT expression increased (Supplemental Fig. 2).

To investigate the source of the trends observed in the gene expression profiles of the acute-phase proteins, we compared their PHx mRNA levels with the cytokine measurements from our previous study under the same experimental conditions (18). We incorporated a time delay to compensate for the delay from the initiation of cytokine signaling to modulation of downstream gene expression. We compared the cytokine measurements at 0, 0.5, and 1 h with the gene expression measurements at 0.5, 1, and 3 h, respectively. The temporal profiles of TNF-α levels showed time-delayed correlation with the temporal profiles of SAA1, representing the acute-phase genes; the Pearson correlation coefficients for both the KO and the WT measurements between TNF-α and SAA1 with the time delay were both positive and very close to 1, indicating a strong linear relationship (Supplemental Fig. 2). The temporal profiles of other cytokines, including IL-6, did not correlate with acute-phase genes in either genotype. In addition to the strong positive correlation observed between TNF-α and the acute-phase genes, the correlation between c-fos and the acute-phase genes was also high, with the Pearson correlation coefficients of 0.89 for the KO and 0.97 for the WT, respectively (data not shown).

Complement and cholesterol metabolism and efflux

In addition to the changes in the early acute-phase genes, the KO transcriptome was enriched for metabolic pathways related to

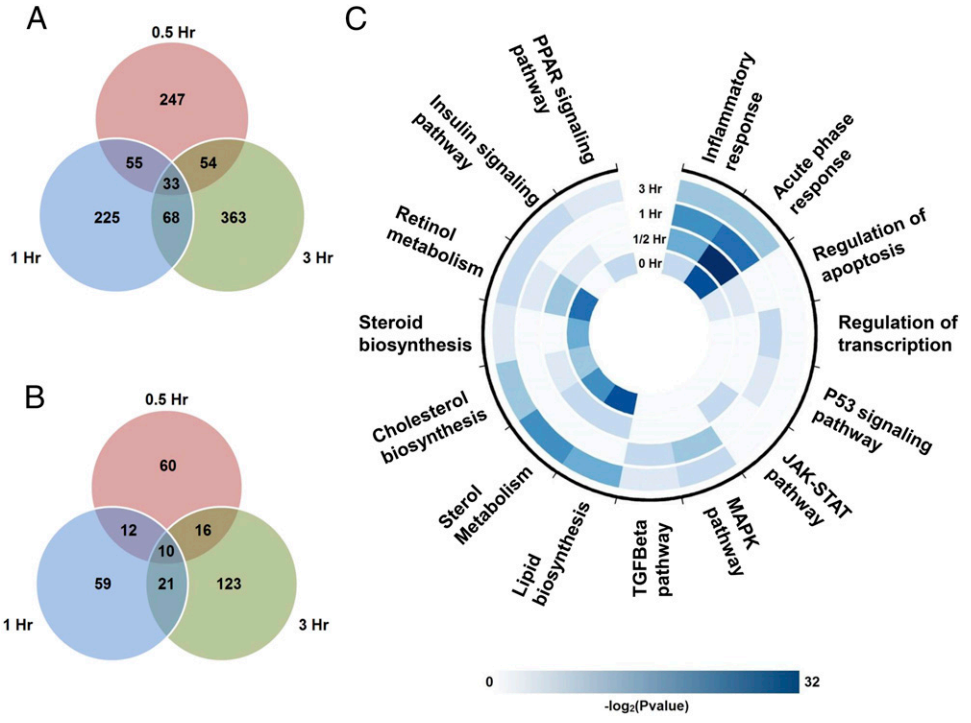

FIGURE 1. Venn diagrams of differentially regulated genes after PHx under the p value cutoff of 0.05 (**A**) and the FDR cutoff of 0.1 (**B**), and overrepresented biological functions and pathways during the priming phase (**C**). (A and B) All data are shown as the number of differentially regulated genes between the KO and the WT at each time point (0.5 h: $n = 8$ mice, 1–3 h: $n = 6$ mice). (C) Enrichment analysis was performed at each time point using DAVID from the list of differentially regulated genes under the p value cutoff of 0.05. Negative $\log_2$ of enrichment p value was used as the scale for the heat map (enrichment $p \leq 0.05$, a modified Fisher exact test from DAVID).

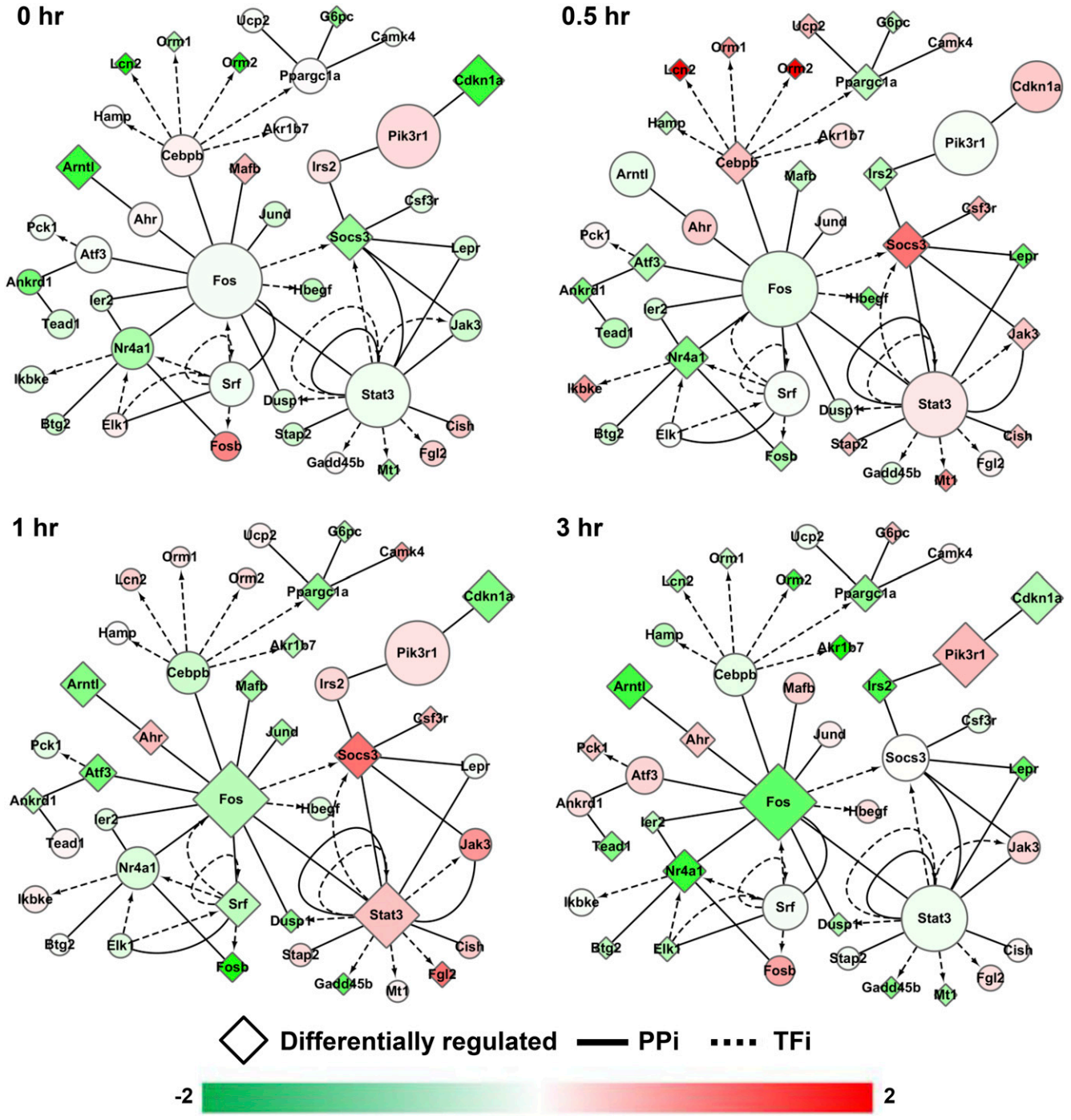

FIGURE 2. Temporal network analysis in Cytoscape. The networks represent the biggest module derived from Autosome clustering at four time points. This particular network of 41 genes shows significant enrichment in transcription (FDR < 0.1, DAVID). Red indicates fold upregulation in the KO, whereas green indicates fold downregulation, with respect to the WT. The size of a node is based on the number of directly connected genes. Solid line indicates protein–protein interaction (PPi), whereas the directed dashed line indicates transcription factor–target interaction (TFi). Diamond shape represents differentially regulated genes, either $p < 0.05$ or FDR < 0.1, at that particular time point between the KO and the WT.

cholesterol metabolism (Fig. 1C). The baseline metabolic changes in the transcriptome also indicated the involvement of complement even before the priming phase of liver regeneration. In the liver, cholesterol homeostasis is closely monitored and regulated by liver X receptor (LXR) that is activated by oxysterols (43). Cholesterol 25-hydroxylase, the gene responsible for the synthesis of the main agonist for LXR, 25-hydroxycholesterol, was significantly downregulated in the KO livers with respect to the WT (Supplemental Fig. 3) (44). Other genes related to cholesterol efflux such as ATP-binding cassette subfamily G (ABCG) member 5 and ABCG8 also showed downregulation (Supplemental Fig. 3) (45). Upregulation of 3-hydroxy-3-methylglutaryl (HMG)-CoA reductase (HMGCR) that results in increased cholesterol biosynthesis was observed at 3 h (Supplemental Fig. 3) (46). These results suggest that cellular conservation of cholesterol is regulated by the complement system during the priming phase of liver regeneration.

To validate the predicted metabolic changes based on the transcriptomic results, we analyzed 143 metabolites using MS. Some notable metabolites related to cholesterol homeostasis were acetyl CoA (acetyl-CoA), HMG-CoA, and CEs (Supplemental Fig. 3).

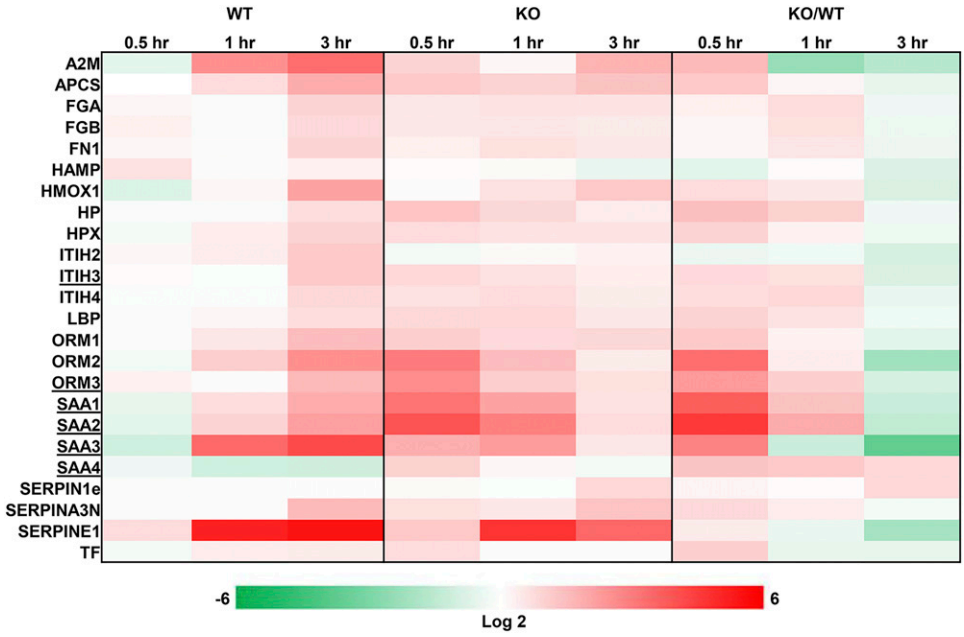

FIGURE 3. Acute-phase genes after PHx. Heat maps of transcriptional changes in the known acute-phase genes are plotted for KO, WT, and KO/WT fold change. Log_2 color scale is used. Underline indicates differentially regulated at all three time points.

Although the changes in these metabolites at 3 h were not statistically significantly different between the KO and the WT livers due to the high variance often observed in metabolic data, their KO/WT fold changes were >1.5. Despite the metabolic and transcriptomic changes related to cholesterol metabolism and efflux, cholesterol levels were fairly consistent across both genotypes at all the time points, consistent with tight control of cellular cholesterol levels during liver regeneration (Supplemental Fig. 3).

Overall metabolic demands

Cellular proliferation can cause significant remodeling of metabolic signals to meet the increased bioenergetic needs of the growing cells, like in cancer (47). Because hepatocytes undergo rapid proliferation during liver regeneration, we compared the metabolic levels between the two genotypes and observed an overall decrease in the KO mice during the late priming phase; 70% of the metabolites showed lower measurements in the KO at 3 h compared with the WT measurements (Fig. 4). Furthermore, 69% of the metabolites that were unrelated to cholesterol homeostasis also showed lower KO measurements (data not shown). These results suggest that metabolic demands in the KO are not being met during the later stage of the priming phase because of the lack of C3 regulation.

To further evaluate metabolic changes, we analyzed the list of differentially regulated genes that may be related to lipid metabolism. The list of 1504 lipid-related mouse genes was taken from the LIPID Metabolites and Pathways Strategy Proteome database (40). A total of 43 genes were differentially regulated at either all three time points or only at 3 h after PHx (Supplemental Fig. 4). Among these genes was peroxisome proliferator-activated receptor γ coactivator 1-α, also known as PGC-1α, a key regulator of energy metabolism (48). In addition, solute carrier family 37 (glucose-6-phosphate transporter) member 1 may also regulate energy metabolism by transporting glycerol-3-phosphate between cellular compartments (49).

Transcriptomic and metabolic changes in the sterol pathway

Correlation analysis between the transcriptomic and the metabolic data was performed for the gene–metabolite pair in the sterol pathway to observe whether the transcriptomic changes would translate into metabolic changes. The majority of the measured gene–metabolite pairs in the sterol pathway showed high correlation (Fig. 5). However, CEs showed significantly different correlation between the genotypes, which suggests that the mechanism for alterations in metabolite levels differ between KO and WT (Fig. 5).

Overall, our results elucidate the role of the complement system in the priming phase of liver regeneration (Fig. 6).

Discussion

Transcriptional regulation of cell cycle–related pathways

The complement system, through activation of C3, regulates several significant genes and pathways related to cell cycle and proliferation, two major processes involved in liver regeneration (12). For example, the complement system activates the MAPK, p53, JAK-STAT, and TGF-β pathways across different time points. In addition, the network analysis shows progressive downregulation of c-fos, an immediate early gene involved in proliferation, in the KO. STAT3 and SOCS3, which are known regulators of liver regeneration, show brief but significant upregulation at one of the time points; STAT3 has been linked with cell survival and DNA synthesis during the acute phase, whereas

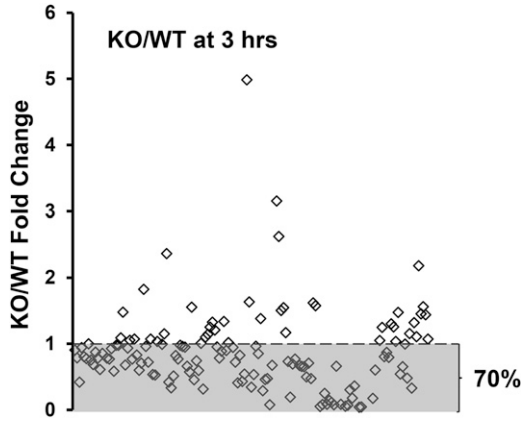

FIGURE 4. Metabolic fold changes at 3 h. KO/WT fold changes at 3 h are shown for all 143 metabolites. Each diamond represents the fold change of a single metabolite.

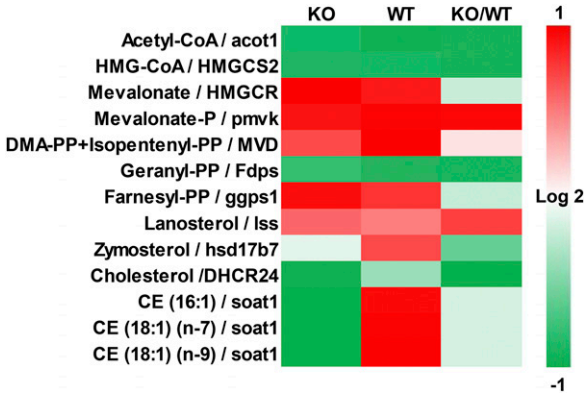

FIGURE 5. Correlation heat map of gene–metabolite pairs in the sterol pathway. Pearson correlation coefficient was calculated for the measured gene–metabolite pairs in the sterol pathway. If multiple genes are known to regulate a metabolite, the pair with the highest correlation was chosen. The numbers of time points used for correlation calculation were 3, 3, and 4 for KO, WT, and KO/WT categories, respectively.

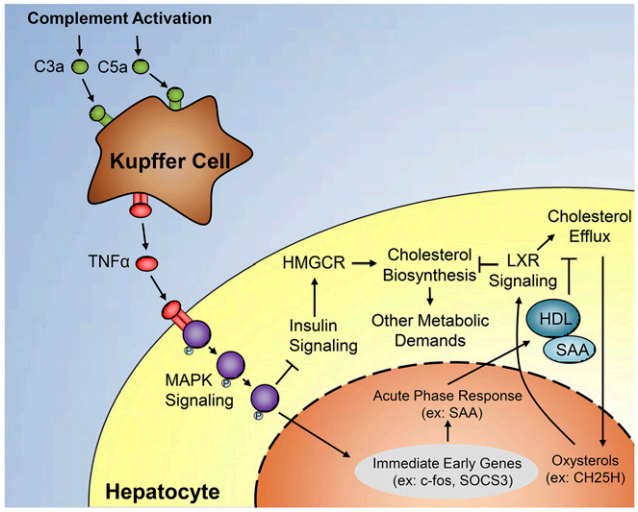

FIGURE 6. The proposed mechanism of the priming phase of complement-induced liver regeneration. Complement activation induced by liver injury or PHx increases the concentration of the complement effector proteins, C3a and C5a, which bind to the nearby Kupffer cells to release TNF-α. TNF-α then binds to the receptors on hepatocytes to initiate the MAPK pathway and its downstream immediate early genes such as c-fos and SOCS3. This leads to activation of acute-phase proteins such as SAA that can replace the lipoprotein of HDL to form acute-phase HDL. Acute-phase HDL promotes lower cholesterol efflux than native HDL, which causes hepatocytes to respond by activating LXR through oxysterols to reduce cholesterol biosynthesis for stable cholesterol levels. TNF-α can also inhibit insulin signaling, potentially through the MAPK pathway, which then reduces the expression of HMGCR, a key enzyme in cholesterol biosynthesis. The reduced cholesterol biosynthesis allows hepatocytes to use their cellular resources to meet other metabolic demands required for upcoming prolonged proliferation of liver regeneration.

SOCS3 negatively regulates liver regeneration by inhibiting the JAK-STAT pathway (50, 51). According to our previous measurements of cytokines on the first 6 h post-PHx, total STAT3 level increased whereas phosphorylation of STAT3 decreased (18). We also observed reduced DNA binding activity of STAT3 during the first 2 h post-PHx (17). These data, when combined together, suggest that reduced STAT3 phosphorylation activation and DNA binding activity may upregulate transcriptomic expression of STAT3 as a compensatory mechanism. Other genes in the transcriptional network did not show clear biological insights because of the observed complexity of the temporal transcriptomic changes.

Transcriptional regulation of the acute-phase genes by TNF-α

The gene expression profiles of the acute-phase proteins such as SAA1, SAA2, ORM2, and ORM3 showed that C3 activation progressively promotes the acute-phase response during the priming phase of liver regeneration. The increased transcriptional regulation of these acute-phase responses at 0.5 h post-PHx in the KO livers also suggest the existence of a compensatory mechanism for the less effective immune response from the complement KO mice. TNF-α, which is regulated by C3a and C5a of the complement system, is the most likely cytokine candidate for regulating the expression of these acute-phase genes because the time-delayed correlation between TNF-α and the acute-phase genes was very high in both the WT and the KO livers (11). In addition, other cytokines, including IL-6, did not result in moderate or high correlation. Furthermore, several studies have shown that TNF-α can regulate acute-phase genes through the MAPK pathway (52, 53). Because the correlation between c-fos and the acute-phase genes was also high in both the WT and the KO livers, TNF-α may regulate the expression of the acute-phase genes through the induction of c-fos and other immediate early genes.

The acute-phase genes and cholesterol efflux

The acute-phase response has been linked with liver cirrhosis, a severe phenotype in advanced liver diseases with impaired liver regeneration (54–56). For example, ORMs and SAAs, the key acute-phase proteins from our results, have been implicated as potential biomarkers for liver cirrhosis in humans (55, 56). These acute-phase proteins showed significantly different transcriptional regulation during the priming phase. We further hypothesized that the acute-phase proteins may regulate cholesterol that is required for cell cycle progression and cell growth. More specifically, the acute-phase proteins may regulate cholesterol efflux through remodeling of high-density lipoprotein (HDL) (57). For example, SAA can remodel native HDL to acute-phase HDL by replacing apolipoprotein A1 as the major apolipoprotein during the acute-phase response (58, 59). Acute-phase HDL with the dominant SAA proteins possesses a lower capacity to promote cholesterol efflux than native HDL; in other words, acute-phase HDL has a higher capacity to keep cholesterol within the cells than the native HDL (60, 61). Because the transcriptional regulations of SAA proteins steadily decreased over time in the KO mice, less SAA proteins were available to remodel native HDL to acute-phase HDL. Higher concentrations of native HDL during the first 3 h is expected to promote higher cholesterol efflux and keep less cholesterol within the cells.

Further evidence for the relationship between SAA-rich acute-phase HDL and the change in cholesterol efflux is total CE delivery. The result from the previous study showed that total CE delivery was significantly higher for acute-phase HDL than for native HDL (60). The metabolic data were consistent with this report; because the concentration of acute-phase HDL decreases over time in the KO, the total CE concentration also decreased significantly from 0.5 to 1 or 3 h. Although the variance of total CE concentration at 0.5 h was high, the majority of CEs with different saturation ratios showed similar profiles.

Regulation of cholesterol metabolism and efflux

Cholesterol is a well-known cell cycle regulator that is tightly controlled by the cells through LXR (62). We hypothesized that if the cholesterol level was to decrease as a result of higher

cholesterol efflux during the first 3 h after PHx, then hepatocytes would respond concomitantly by transcriptionally increasing cholesterol biosynthesis and reducing its catabolism and secretion. Several of our results support this hypothesis. For example, significant downregulation of cholesterol 25-hydroxylase that is responsible for synthesizing 25-hydroxycholesterol was observed at 3 h. This oxysterol is the main agonist of LXR; it can deactivate the LXR pathway and downregulate genes related to cholesterol efflux such as ATP-binding cassette subfamily G member 5 (ABCG5) and ATP-binding cassette subfamily G member 8 (ABCG8) (44, 45). Hepatocytes also stimulated the expression of HMGCR at 3 h post-PHx to promote cholesterol biosynthesis to further restore cholesterol availability (46). Upregulation of HMGCR can be explained by the reduced concentration of TNF-α, an inhibitor of the insulin signaling pathway, because insulin can strongly stimulate HMGCR synthesis (63, 64). Further evidence for increased cholesterol availability within hepatocytes in the KO was enriched steroid and bile acid biosynthesis at 3 h from the enrichment analysis of the transcriptomic data.

As a result of transcriptional regulation of cholesterol metabolism and efflux, which can restore the cholesterol availability lowered by the native HDL during the first 3 h, the cholesterol level remained relatively stable in both genotypes across all time points. This highlights the tight regulation of cholesterol by hepatocytes to ensure successful progression of the cell cycle during the priming phase of liver regeneration. Although the resulting cholesterol level did not change much across the genotypes during the priming phase, it may change during the later stages of liver regeneration, such as in the proliferation phase, where significant metabolic changes are known to occur. Moreover, most of the metabolites and their associated genes in the sterol pathway showed high correlation, suggesting that the transcriptomic changes are being translated into metabolic changes.

Metabolic demands during early liver regeneration

Besides cholesterol metabolism, the complement system may help hepatocytes meet other metabolic demands. For example, the majority of the 143 measured metabolites showed lower measurements in KO livers compared with WT at 3 h post-PHx. This result did not change when the metabolites that were related to cholesterol metabolism were excluded. Based on these results, we hypothesize that when KO hepatocytes are focused on synthesizing cholesterol and lowering its secretion, fewer resources are made available to meet the other metabolic needs in preparation for prolonged cellular proliferation. A similar phenomenon occurs in cancer cells when they dramatically alter the metabolic circuitry to meet the bioenergetic and biosynthetic demands of increased proliferation (47, 65). Our data also showed that peroxisome proliferator-activated receptor γ coactivator 1-α, the gene involved in energy metabolism, and solute carrier family 37 (glucose-6-phosphate transporter) member 1, the gene involved in transporting glycerol-3-phosphate, are differentially regulated at all three time points. The regenerative process is highly dependent on increased proliferation, and liver regeneration is no exception.

A systems overview

In this study, we have performed systems analyses using diverse measurements across multiple time points to investigate the complex mechanism of the priming phase of complement-induced liver regeneration. Based on the significant results, we have proposed a mechanistic relationship between the complement activation at the level C3, acute-phase proteins, and cholesterol metabolism during the priming phase of liver regeneration (Fig. 6). Future studies including proteomic analysis and investigation of the role of the complement system using genetic and pharmacological perturbations on the later stages of liver regeneration can supplement the findings of this study.

Disclosures

The authors have no financial conflicts of interest.

References

1. Clavien, P. A. 2008. Liver regeneration: a spotlight on the novel role of platelets and serotonin. *Swiss Med. Wkly.* 138: 361–370.
2. Clavien, P. A., H. Petrowsky, M. L. DeOliveira, and R. Graf. 2007. Strategies for safer liver surgery and partial liver transplantation. *N. Engl. J. Med.* 356: 1545–1559.
3. Gotohda, N., H. Iwagaki, M. Ozaki, T. Kinoshita, M. Konishi, T. Nakagohri, S. Takahashi, S. Saito, T. Yagi, and N. Tanaka. 2008. Deficient response of IL-6 impaired liver regeneration after hepatectomy in patients with viral hepatitis. *Hepatogastroenterology* 55: 1439–1444.
4. Hines, I. N., M. Kremer, F. Isayama, A. W. Perry, R. J. Milton, A. L. Black, C. L. Byrd, and M. D. Wheeler. 2007. Impaired liver regeneration and increased oval cell numbers following T cell-mediated hepatitis. *Hepatology* 46: 229–241.
5. Tanemura, A., S. Mizuno, H. Wada, T. Yamada, T. Nobori, and S. Isaji. 2012. Donor age affects liver regeneration during early period in the graft liver and late period in the remnant liver after living donor liver transplantation. *World J. Surg.* 36: 1102–1111.
6. Torbenson, M., S. Q. Yang, H. Z. Liu, J. Huang, W. Gage, and A. M. Diehl. 2002. STAT-3 overexpression and p21 up-regulation accompany impaired regeneration of fatty livers. *Am. J. Pathol.* 161: 155–161.
7. Yang, S. Q., H. Z. Lin, A. K. Mandal, J. Huang, and A. M. Diehl. 2001. Disrupted signaling and inhibited regeneration in obese mice with fatty livers: implications for nonalcoholic fatty liver disease pathophysiology. *Hepatology* 34: 694–706.
8. Michalopoulos, G. K. 2010. Liver regeneration after partial hepatectomy: critical analysis of mechanistic dilemmas. *Am. J. Pathol.* 176: 2–13.
9. Zimmermann, A. 2004. Regulation of liver regeneration. *Nephrol. Dial. Transplant.* 19(Suppl. 4): iv6–iv10.
10. Su, A. I., L. G. Guidotti, J. P. Pezacki, F. V. Chisari, and P. G. Schultz. 2002. Gene expression during the priming phase of liver regeneration after partial hepatectomy in mice. *Proc. Natl. Acad. Sci. USA* 99: 11181–11186.
11. DeAngelis, R. A., M. M. Markiewski, and J. D. Lambris. 2006. Liver regeneration: a link to inflammation through complement. *Adv. Exp. Med. Biol.* 586: 17–34.
12. Taub, R. 2004. Liver regeneration: from myth to mechanism. *Nat. Rev. Mol. Cell Biol.* 5: 836–847.
13. Grisham, J. W. 1962. A morphologic study of deoxyribonucleic acid synthesis and cell proliferation in regenerating rat liver; autoradiography with thymidine-H3. *Cancer Res.* 22: 842–849.
14. Nygård, I. E., K. E. Mortensen, J. Hedegaard, L. N. Conley, T. Kalstad, C. Bendixen, and A. Revhaug. 2012. The genetic regulation of the terminating phase of liver regeneration. *Comp. Hepatol.* 11: 3.
15. DeAngelis, R. A., M. M. Markiewski, I. Kourtzelis, S. Rafail, M. Syriga, A. Sandor, M. R. Maurya, S. Gupta, S. Subramaniam, and J. D. Lambris. 2012. A complement-IL-4 regulatory circuit controls liver regeneration. *J. Immunol.* 188: 641–648.
16. Mastellos, D., J. C. Papadimitriou, S. Franchini, P. A. Tsonis, and J. D. Lambris. 2001. A novel role of complement: mice deficient in the fifth component of complement (C5) exhibit impaired liver regeneration. *J. Immunol.* 166: 2479–2486.
17. Strey, C. W., M. Markiewski, D. Mastellos, R. Tudoran, L. A. Spruce, L. E. Greenbaum, and J. D. Lambris. 2003. The proinflammatory mediators C3a and C5a are essential for liver regeneration. *J. Exp. Med.* 198: 913–923.
18. Markiewski, M. M., R. A. DeAngelis, C. W. Strey, P. G. Foukas, C. Gerard, N. Gerard, R. A. Wetsel, and J. D. Lambris. 2009. The regulation of liver cell survival by complement. *J. Immunol.* 182: 5412–5418.
19. Higgins, G. A. R. 1932. Experimental pathology of the liver 1. Restoration of the liver of the white rat following partial surgical removal. *Arch. Pathol. (Chic.)* 12: 186–202.
20. Sun, R., O. Park, N. Horiguchi, S. Kulkarni, W. I. Jeong, H. Y. Sun, S. Radaeva, and B. Gao. 2006. STAT1 contributes to dsRNA inhibition of liver regeneration after partial hepatectomy in mice. *Hepatology* 44: 955–966.
21. Desbois-Mouthon, C., D. Wendum, A. Cadoret, C. Rey, P. Leneuve, A. Blaise, C. Housset, F. Tronche, Y. Le Bouc, and M. Holzenberger. 2006. Hepatocyte proliferation during liver regeneration is impaired in mice with liver-specific IGF-1R knockout. *FASEB J.* 20: 773–775.
22. Hu, J., H. Ge, M. Newman, and K. Liu. 2012. OSA: a fast and accurate alignment tool for RNA-Seq. *Bioinformatics* 28: 1933–1934.
23. Anders, S., P. T. Pyl, and W. Huber. 2015. HTSeq–a Python framework to work with high-throughput sequencing data. *Bioinformatics* 31: 166–169.
24. Anders, S., and W. Huber. 2010. Differential expression analysis for sequence count data. *Genome Biol.* 11: R106.
25. Spandidos, A., X. Wang, H. Wang, and B. Seed. 2010. PrimerBank: a resource of human and mouse PCR primer pairs for gene expression detection and quantification. *Nucleic Acids Res.* 38: D792–D799.
26. Wang, X., A. Spandidos, H. Wang, and B. Seed. 2012. PrimerBank: a PCR primer database for quantitative gene expression analysis, 2012 update. *Nucleic Acids Res.* 40: D1144–D1149.

27. Huang, W., B. T. Sherman, and R. A. Lempicki. 2009. Systematic and integrative analysis of large gene lists using DAVID bioinformatics resources. *Nat. Protoc.* 4: 44–57.
28. Krzywinski, M., J. Schein, I. Birol, J. Connors, R. Gascoyne, D. Horsman, S. J. Jones, and M. A. Marra. 2009. Circos: an information aesthetic for comparative genomics. *Genome Res.* 19: 1639–1645.
29. Shannon, P., A. Markiel, O. Ozier, N. S. Baliga, J. T. Wang, D. Ramage, N. Amin, B. Schwikowski, and T. Ideker. 2003. Cytoscape: a software environment for integrated models of biomolecular interaction networks. *Genome Res.* 13: 2498–2504.
30. Stark, C., B. J. Breitkreutz, T. Reguly, L. Boucher, A. Breitkreutz, and M. Tyers. 2006. BioGRID: a general repository for interaction datasets. *Nucleic Acids Res.* 34: D535–D539.
31. Szklarczyk, D., A. Franceschini, M. Kuhn, M. Simonovic, A. Roth, P. Minguez, T. Doerks, M. Stark, J. Muller, P. Bork, et al. 2011. The STRING database in 2011: functional interaction networks of proteins, globally integrated and scored. *Nucleic Acids Res.* 39: D561–D568.
32. von Mering, C., M. Huynen, D. Jaeggi, S. Schmidt, P. Bork, and B. Snel. 2003. STRING: a database of predicted functional associations between proteins. *Nucleic Acids Res.* 31: 258–261.
33. Wingender, E., X. Chen, R. Hehl, H. Karas, I. Liebich, V. Matys, T. Meinhardt, M. Prüss, I. Reuter, and F. Schacherer. 2000. TRANSFAC: an integrated system for gene expression regulation. *Nucleic Acids Res.* 28: 316–319.
34. Morris, J. H., L. Apeltsin, A. M. Newman, J. Baumbach, T. Wittkop, G. Su, G. D. Bader, and T. E. Ferrin. 2011. clusterMaker: a multi-algorithm clustering plugin for Cytoscape. *BMC Bioinformatics* 12: 436.
35. Newman, A. M., and J. B. Cooper. 2010. AutoSOME: a clustering method for identifying gene expression modules without prior knowledge of cluster number. *BMC Bioinformatics* 11: 117.
36. Overmyer, K. A., C. Thonusin, N. R. Qi, C. F. Burant, and C. R. Evans. 2015. Impact of anesthesia and euthanasia on metabolomics of mammalian tissues: studies in a C57BL/6J mouse model. *PLoS One* 10: e0117232.
37. Begley, P., S. Francis-McIntyre, W. B. Dunn, D. I. Broadhurst, A. Halsall, A. Tseng, J. Knowles, R. Goodacre, and D. B. Kell, HUSERMET Consortium. 2009. Development and performance of a gas chromatography–time-of-flight mass spectrometry analysis for large-scale nontargeted metabolomic studies of human serum. *Anal. Chem.* 81: 7038–7046.
38. Bligh, E. G., and W. J. Dyer. 1959. A rapid method of total lipid extraction and purification. *Can. J. Biochem. Physiol.* 37: 911–917.
39. Morrison, W. R., and L. M. Smith. 1964. Preparation of fatty acid methyl esters and dimethylacetals from lipids with boron fluoride–methanol. *J. Lipid Res.* 5: 600–608.
40. Subramaniam, S., E. Fahy, S. Gupta, M. Sud, R. W. Byrnes, D. Cotter, A. R. Dinasarapu, and M. R. Maurya. 2011. Bioinformatics and systems biology of the lipidome. *Chem. Rev.* 111: 6452–6490.
41. Dennis, E. A., R. A. Deems, R. Harkewicz, O. Quehenberger, H. A. Brown, S. B. Milne, D. S. Myers, C. K. Glass, G. Hardiman, D. Reichart, et al. 2010. A mouse macrophage lipidome. *J. Biol. Chem.* 285: 39976–39985.
42. Ingenuity Target Explorer. 2015. QIAGEN. Available at: https://targetexplorer.ingenuity.com. Accessed: October 19, 2015.
43. Hu, Y. W., L. Zheng, and Q. Wang. 2010. Regulation of cholesterol homeostasis by liver X receptors. *Clin. Chim. Acta* 411: 617–625.
44. Chen, W., G. Chen, D. L. Head, D. J. Mangelsdorf, and D. W. Russell. 2007. Enzymatic reduction of oxysterols impairs LXR signaling in cultured cells and the livers of mice. *Cell Metab.* 5: 73–79.
45. Repa, J. J., K. E. Berge, C. Pomajzl, J. A. Richardson, H. Hobbs, and D. J. Mangelsdorf. 2002. Regulation of ATP-binding cassette sterol transporters ABCG5 and ABCG8 by the liver X receptors alpha and beta. *J. Biol. Chem.* 277: 18793–18800.
46. Jo, Y., and R. A. Debose-Boyd. 2010. Control of cholesterol synthesis through regulated ER-associated degradation of HMG CoA reductase. *Crit. Rev. Biochem. Mol. Biol.* 45: 185–198.
47. Phan, L. M., S. C. Yeung, and M. H. Lee. 2014. Cancer metabolic reprogramming: importance, main features, and potentials for precise targeted anti-cancer therapies. *Cancer Biol. Med.* 11: 1–19.
48. Liang, H., and W. F. Ward. 2006. PGC-1alpha: a key regulator of energy metabolism. *Adv. Physiol. Educ.* 30: 145–151.
49. Bartoloni, L., M. Wattenhofer, J. Kudoh, A. Berry, K. Shibuya, K. Kawasaki, J. Wang, S. Asakawa, I. Talior, B. Bonne-Tamir, et al. 2000. Cloning and characterization of a putative human glycerol 3-phosphate permease gene (SLC37A1 or G3PP) on 21q22.3: mutation analysis in two candidate phenotypes, DFNB10 and a glycerol kinase deficiency. *Genomics* 70: 190–200.
50. Moh, A., Y. Iwamoto, G. X. Chai, S. S. Zhang, A. Kano, D. D. Yang, W. Zhang, J. Wang, J. J. Jacoby, B. Gao, et al. 2007. Role of STAT3 in liver regeneration: survival, DNA synthesis, inflammatory reaction and liver mass recovery. *Lab. Invest.* 87: 1018–1028.
51. Riehle, K. J., J. S. Campbell, R. S. McMahan, M. M. Johnson, R. P. Beyer, T. K. Bammler, and N. Fausto. 2008. Regulation of liver regeneration and hepatocarcinogenesis by suppressor of cytokine signaling 3. *J. Exp. Med.* 205: 91–103.
52. Thorn, C. F., Z. Y. Lu, and A. S. Whitehead. 2004. Regulation of the human acute phase serum amyloid A genes by tumour necrosis factor-alpha, interleukin-6 and glucocorticoids in hepatic and epithelial cell lines. *Scand. J. Immunol.* 59: 152–158.
53. Westra, J., J. Bijzet, B. Doornbos-van der Meer, M. H. van Rijswijk, and P. C. Limburg. 2006. Differential influence of p38 mitogen activated protein kinase (MAPK) inhibition on acute phase protein synthesis in human hepatoma cell lines. *Ann. Rheum. Dis.* 65: 929–935.
54. Lemmers, A., T. Gustot, A. Durnez, S. Evrard, C. Moreno, E. Quertinmont, V. Vercruysse, P. Demetter, D. Franchimont, O. Le Moine, et al. 2009. An inhibitor of interleukin-6 trans-signalling, sgp130, contributes to impaired acute phase response in human chronic liver disease. *Clin. Exp. Immunol.* 156: 518–527.
55. Sasaki, M., N. Yoneda, S. Kitamura, Y. Sato, and Y. Nakanuma. 2012. A serum amyloid A-positive hepatocellular neoplasm arising in alcoholic cirrhosis: a previously unrecognized type of inflammatory hepatocellular tumor. *Mod. Pathol.* 25: 1584–1593.
56. Rydén, I., P. Påhlsson, and S. Lindgren. 2002. Diagnostic accuracy of alpha(1)-acid glycoprotein fucosylation for liver cirrhosis in patients undergoing hepatic biopsy. *Clin. Chem.* 48: 2195–2201.
57. O'Brien, K. D., and A. Chait. 2006. Serum amyloid A: the "other" inflammatory protein. *Curr. Atheroscler. Rep.* 8: 62–68.
58. Coetzee, G. A., A. F. Strachan, D. R. van der Westhuyzen, H. C. Hoppe, M. S. Jeenah, and F. C. de Beer. 1986. Serum amyloid A-containing human high density lipoprotein 3. Density, size, and apolipoprotein composition. *J. Biol. Chem.* 261: 9644–9651.
59. de Beer, M. C., N. R. Webb, J. M. Wroblewski, V. P. Noffsinger, D. L. Rateri, A. Ji, D. R. van der Westhuyzen, and F. C. de Beer. 2010. Impact of serum amyloid A on high density lipoprotein composition and levels. *J. Lipid Res.* 51: 3117–3125.
60. Artl, A., G. Marsche, S. Lestavel, W. Sattler, and E. Malle. 2000. Role of serum amyloid A during metabolism of acute-phase HDL by macrophages. *Arterioscler. Thromb. Vasc. Biol.* 20: 763–772.
61. Jahangiri, A., M. C. de Beer, V. Noffsinger, L. R. Tannock, C. Ramaiah, N. R. Webb, D. R. van der Westhuyzen, and F. C. de Beer. 2009. HDL remodeling during the acute phase response. *Arterioscler. Thromb. Vasc. Biol.* 29: 261–267.
62. Kim, K. H., G. Y. Lee, J. I. Kim, M. Ham, J. Won Lee, and J. B. Kim. 2010. Inhibitory effect of LXR activation on cell proliferation and cell cycle progression through lipogenic activity. *J. Lipid Res.* 51: 3425–3433.
63. Peraldi, P., G. S. Hotamisligil, W. A. Buurman, M. F. White, and B. M. Spiegelman. 1996. Tumor necrosis factor (TNF)-alpha inhibits insulin signaling through stimulation of the p55 TNF receptor and activation of sphingomyelinase. *J. Biol. Chem.* 271: 13018–13022.
64. Osborne, A. R., V. V. Pollock, W. R. Lagor, and G. C. Ness. 2004. Identification of insulin-responsive regions in the HMG-CoA reductase promoter. *Biochem. Biophys. Res. Commun.* 318: 814–818.
65. Jones, R. G., and C. B. Thompson. 2009. Tumor suppressors and cell metabolism: a recipe for cancer growth. *Genes Dev.* 23: 537–548.